PHYSICAL REVIEW B **85**, 085121 (2012)

Symmetry breaking via orbital-dependent reconstruction of electronic structure in detwinned NaFeAs

Y. Zhang,[1] C. He,[1] Z. R. Ye,[1] J. Jiang,[1] F. Chen,[1] M. Xu,[1] Q. Q. Ge,[1] B. P. Xie,[1] J. Wei,[2] M. Aeschlimann,[2] X. Y. Cui,[3] M. Shi,[3] J. P. Hu,[4] and D. L. Feng[1,*]

[1]*State Key Laboratory of Surface Physics, Key Laboratory of Micro and Nano Photonic Structures (MOE), and Department of Physics, Fudan University, Shanghai 200433, People's Republic of China*

[2]*Fachbereich Physik and Research Center OPTIMAS, Technische Universitaet Kaiserslautern, Kaiserslautern, 67663, Germany*

[3]*Swiss Light Source, Paul-Scherrer Institut, 5232 Villigen, Switzerland*

[4]*Department of Physics, Purdue University, West Lafayette, Indiana 47907, USA*

(Received 5 December 2011; published 22 February 2012)

The superconductivity discovered in iron pnictides is intimately related to a nematic ground state, where the C_4 rotational symmetry is broken via the structural and magnetic transitions. We here study the nematicity in NaFeAs with polarization-dependent angle-resolved photoemission spectroscopy. A uniaxial pressure was applied on the sample to overcome the twinning effect in the low temperature C_2-symmetric state and obtain a much simpler electronic structure than that of a twinned sample. We found the electronic structure undergoes an orbital-dependent reconstruction in the nematic state, primarily involving the d_{xy}- and d_{yz}-dominated bands. These bands strongly hybridize with each other, inducing a band splitting, while the d_{xz}-dominated bands only exhibit an energy shift without any reconstruction. These findings suggest that the spin fluctuations at high temperatures and their coupling with the orbital degree of freedom could be the dominant force to drive the nematicity, while the ferro-orbital ordering between d_{xz} and d_{yz} orbitals can only play a minor role here.

DOI: 10.1103/PhysRevB.85.085121 PACS number(s): 74.25.Jb, 74.70.Xa, 79.60.−i

I. INTRODUCTION

The parent compounds of iron pnictides share a common spin density wave or collinear antiferromagnetic (CAF) state, which is characterized by a ferromagnetic (FM) spin alignment along one direction in the two-dimensional rectangular lattice formed by iron sites and an antiferromagnetic (AFM) spin alignment along the other direction.[1–3] Superconductivity in iron pnictides emerges when the magnetic order is suppressed through chemical substitution or physical pressure.[4–6] The mechanism causing the CAF order thus may be intimately related to the superconductivity.

The development of the CAF order is always accompanied by a lattice structure distortion, more specifically, a tetragonal-to-orthorhombic structural distortion. The transition temperature (T_S) at which the lattice distortion takes place either precedes or coincides with the CAF Neel transition temperature (T_N).[1–3] The coincidence between the two transitions can be understood from a simple symmetry analysis. Besides breaking magnetic symmetry, the CAF state also breaks C_4 lattice symmetry of the tetragonal lattice. This lattice symmetry breaking due to the magnetic configuration can be attributed solely to the development of a nematic electronic order that only accounts for the rotational symmetry breaking but not to the broken magnetic symmetry. Based on the textbook Ginzburg-Laudau approach, the orthorhombic lattice distortion breaks the same C_4 lattice symmetry. Therefore, the nematic electronic order and the orthorhombic lattice distortion are allowed by symmetry to be coupled with each other. Since the observed lattice distortion in all families of iron pnictides is rather small, the electronic nematism could be dominant.

So far, there are many experimental evidences supporting the dominance of the electronic nematic behavior in iron pnictides. Transport and neutron scattering measurements found a strong in-plane anisotropy of the resistivity and magnetic excitations.[7–10] Angle-resolved photoemission spectroscopy (ARPES), scanning tunneling microscopy, and quantum oscillation studies further revealed a complex electronic structure with C_2 rotational symmetry.[11–15] Moreover, the Fermi surface was suggested to be orbital polarized with almost pure d_{xz} orbital character[16] in the CAF state. The energy splitting of the d_{xz}- and d_{yz}-dominated bands was further observed far above T_N.[12] The observation of such a ferro-orbital ordering has led to a strong debate on the origin of the nematism: whether the electronic nematicity stems from the magnetic or orbital degree of freedom. Theoretically, some suggest that the nematicity is originated from spin fluctuations,[17–19] while others suggest the CAF state comes from a ferro-orbital ordering.[20–23] Although following the symmetry argument that the electronic nematicities from both origins must be coupled to each other, direct experimental evidence is needed to answer how strongly such a coupling is, and whether one is dominant over the other.

Previous ARPES studies mainly focus on the so-called "122" series of iron pnictides, such as $BaFe_{2-x}Co_xAs_2$ and $CaFe_2As_2$. Although the mechanically detwinning methods were used to avoid the complexity due to the twinning effect in the CAF state, the observed electronic structures are still very complicated.[11–13] It is thus difficult to obtain a comprehensive understanding of the complex electronic structure and its orbital character in the nematic state. In this paper, we report a systematic ARPES study on detwinned NaFeAs. The observed electronic structure is much simpler than those of the 122 series. Because of the polarization-sensitivity of orbitals in photoemission experiment, we could selectively probe the bands with different orbital characters. We found that the C_4

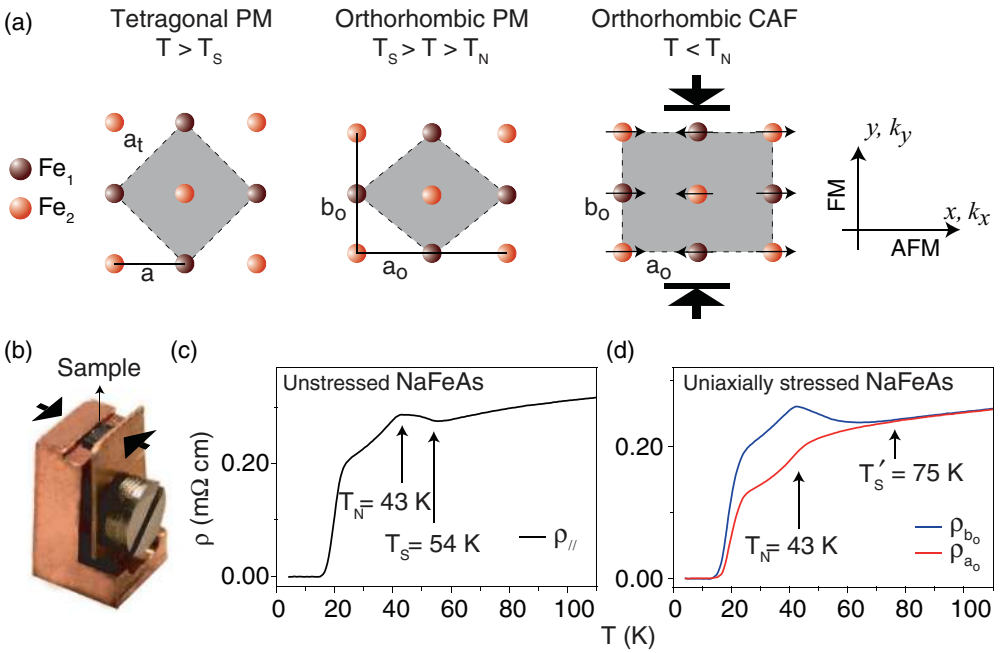

FIG. 1. (Color online) (a) Cartoon of the lattice and spin structure in tetragonal PM, orthorhombic PM, and orthorhombic CAF state. The x and y axes are defined along the iron-iron directions. The black arrows show the direction of the uniaxial pressure applied in the mechanical detwinning process. (b) The photograph of the device used to detwin the samples in our experiments. (c), (d) The temperature-dependent resistivity of unstressed and uniaxially stressed NaFeAs, respectively.

rotational symmetry of the electronic structure is broken via band reconstruction and the band reconstruction itself is also strongly orbital-dependent: the d_{xy}- and d_{yz}-dominated bands open a large hybridization gap at all the band crossings, while the d_{xz}-dominated bands only exhibit an energy shift without any reconstruction. Moreover, the observed total occupation of d_{xz} is almost invariant. These results suggest that the ferro-orbital ordering between d_{xz} and d_{yz} can only play a very limited role in driving the electronic nematicity. On the other hand, the orbital weight redistribution involving the d_{yz} and d_{xy} orbitals could be explained through an orbital-dependent spin polarization far above the Neel transition temperature, which suggests that the nematic spin fluctuations at high temperatures and their coupling with orbital degree of freedom could be the driving force for the nematic electronic state in iron pnictides.

II. EXPERIMENTAL

NaFeAs single crystals were synthesized by a self-flux method.[24] Similar to other parent compounds of iron pnictides, the high temperature phase ($T > T_S$) is in a tetragonal paramagnetic (PM) state, where each unit cell has two irons due to the inequivalent positions of arsenic ions in the FeAs layer [Fig. 1(a)]. Through the structural transition ($a_o > b_o$), there is an orthorhombic PM state ($T_S > T > T_N$) with C_2 rotational symmetry. The CAF magnetic order shows up when entering the orthorhombic CAF state ($T < T_N$).[1–3] The x or k_x axes and y or k_y axes are defined along the AFM and FM directions, respectively. Previous ARPES study on NaFeAs observed a complex electronic structure in the orthorhombic CAF state due to twinned domains of the sample.[24] Taking the advantage of the mechanically detwinning method,[8,25] single domain with sufficiently large size was achieved in our experiment by applying uniaxial pressure along Fe-Fe direction [Figs. 1(a) and 1(b)]. As a result, we could investigate the electronic structure of the orthorhombic CAF state without the complexity of twinning.

The temperature-dependent resistivity of unstressed sample is consistent with the neutron scattering and transport measurements.[3,26] There are two inflexion points at 54 and 43 K, corresponding to the structural transition temperature (T_S) and the Neel transition temperature (T_N), respectively [Fig. 1(c)]. Superconductivity shows up at 20 K, which might be due to the doping effect of the deficient or excess sodium ions. When a uniaxial pressure is applied, the in-plane anisotropy of the resistivity ($\rho_{b_o} > \rho_{a_o}$) emerges at about 75 K, much higher than T_S and T_N in the unstressed sample [Fig. 1(d)]. Similar behavior has been reported in 122 series.[8–10] Recent neutron and x-ray scattering experiments have pointed out that the in-plane anisotropy of the resistivity in detwinned $BaFe_2As_2$ could be related to the lattice distortion.[27,28] The applied uniaxial pressure or strain could smear the structural transition and increase the onset temperature of the lattice distortion. Therefore, we attribute the 75 K observed here to be the structural transition temperature (T_S') in uniaxially stressed samples.

ARPES studies were performed at the SIS beamline of the Swiss Light Source (SLS). All the data were taken with a Scienta R4000 electron analyzer, the overall energy resolution was 15 meV and the angular resolution was 0.3 degree. The samples were cleaved *in situ* and measured under ultra-high vacuum of 5×10^{-11} torr. The polarization-sensitivity of orbitals in ARPES is a powerful tool to identify the orbital characters

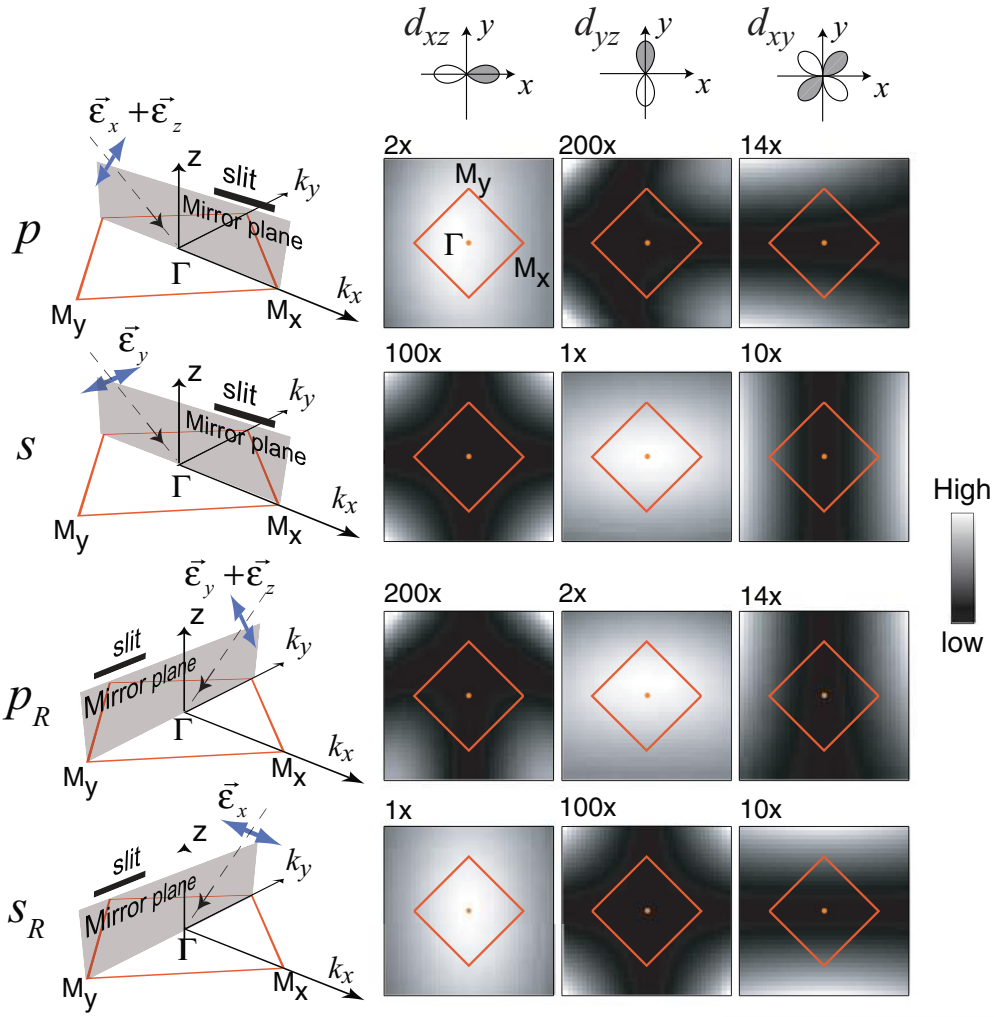

FIG. 2. (Color online) The experimental setup and matrix element calculations for three 3*d* orbitals. The mirror planes are defined by the analyzer slit and the sample surface normal. The two-dimensional plot of the Brillouin zone of NaFeAs is illustrated by red solid squares. Note that the photoemission cross-sections are amplified by a factor shown at the upper-left corner of the panels. Thus, all the panels could be shown in the same color scales. There is a minor asymmetry in certain distributions caused by the out-of-plane component of the polarization.

of band structure.[29,30] The photoemission intensity is proportional to the matrix element of the photoemission process $|M^{\mathbf{k}}_{f,i}|$, which can be described by $|M^{\mathbf{k}}_{f,i}| \propto |\langle \phi^{\mathbf{k}}_f | \hat{\varepsilon} \cdot \mathbf{r} | \phi^{\mathbf{k}}_i \rangle|^2$, where $\hat{\varepsilon}$ is the unit vector of the electric field of the light, and $\phi^{\mathbf{k}}_i$ is the initial-state wave function. For high kinetic-energy photoelectrons, the final-state wave function $\phi^{\mathbf{k}}_f$ can be approximated by a plane-wave state $e^{i\mathbf{k}\cdot\mathbf{r}}$ with $\mathbf{k}$ in the mirror plane. By rotating the polarization of incoming photons or the azimuth angle of the sample, four experimental geometries could be achieved named as p, s, p_R, and s_R, respectively (Fig. 2). The subscript "R" stands for the rotation of the sample. Since the low-lying electronic structures at the Fermi energy (E_F) of iron pnictides are commonly believed to be mostly composed of the d_{xz}, d_{yz}, and d_{xy} orbitals,[31] the matrix element distributions for these three orbitals were calculated in four geometries. As shown in Fig. 2, the matrix element distributions of the d_{xz} and d_{yz} orbitals exhibit a strong polarization dependence throughout the first Brillouin zone, reflecting the opposite symmetry of these two orbitals. The matrix element distribution of d_{xy} is suppressed along the direction parallel to the in-plane component of the polarization, due to its odd spatial symmetry with respect to the mirror planes.

III. THE ELECTRONIC STRUCTURE IN THE TETRAGONAL PARAMAGNETIC STATE

Based on previous studies,[24,32] Fig. 3(a) sketches the Fermi surface of NaFeAs, which consists of two hole pockets (α and β) around the zone center (Γ) and two electron pockets (η and δ) around the zone corner (M) in the tetragonal PM state. The orbital characters are dominated by the d_{xz}, d_{yz}, and d_{xy} orbitals.[33] The distribution of d_{xz} is equivalent to that of the d_{yz} orbital after rotating 90 degrees, which is protected by the C_4 rotational symmetry in the tetragonal PM state. For simplicity, the continuous orbital evolution on the Fermi surface and the orbital mixing on the bands are not illustrated here, which should be finite due to the hybridization of the bands with different orbitals. According to the calculation in Sec. II, we could predict the observable Fermi surfaces in different geometries as shown in Fig. 3(b). The

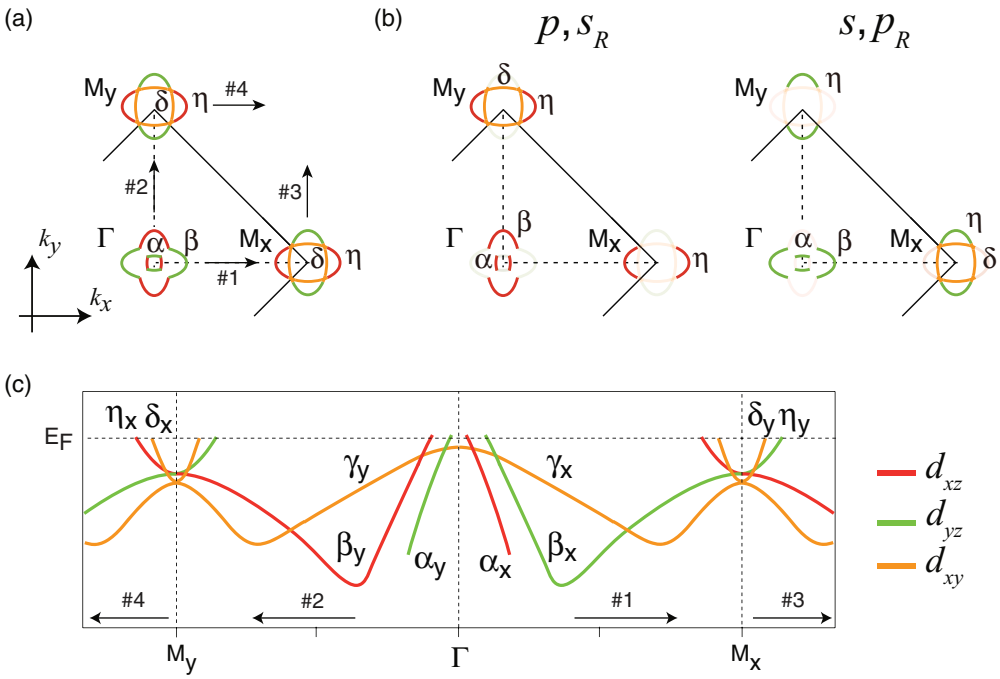

FIG. 3. (Color online) The sketch of the low-lying electronic structure of NaFeAs in the tetragonal PM state. (a) The sketch of the Fermi surface and its orbital character in the folded Brillouin zone for two iron ions per unit cell (solid lines) in the tetragonal PM state. (b) The observable Fermi surfaces in different experimental geometries. (c) The electronic structure of NaFeAs near E_F in the tetragonal PM state.

polarization dependence of the Fermi surface is only sensitive to the in-plane component of the polarization. The low-lying electronic structure of NaFeAs is illustrated in Fig. 3(c). The bands dispersed along k_x and k_y directions are distinguished with the "x" and "y" subscripts here and throughout the paper. As shown by the band calculation,[31] the β_x and γ_x bands should connect with the band bottoms of η_y and δ_y at the M point, respectively, which is guaranteed by the continuous evolution of bands in the unfolded Brillouin zone for one iron ion per unit cell. Note that, since the electronic structure of NaFeAs shows little k_z dependence[33] in both the tetragonal PM and CAF states, we only consider a two-dimensional electronic structure hereafter.

To further confirm the orbital character of the electronic structure, the photoemission intensity maps obtained in the p and s geometries are compared in Fig. 4(a). Around Γ, the photoemission intensity distribution rotates 90 degrees from p to s geometry, which is consistent with the predicted distribution of the d_{xz} and d_{yz} orbitals on the α and β hole pockets. The electron pockets are observed either around M_y in the p geometry or around M_x in the s geometry, which correspond to the δ electron pockets dominated by the d_{xy} orbital. We did not observe the η electron pocket here, which could be due to particular photon energy or experimental setup, since the outer η electron pockets could be observed in previous studies[24] or with 118 eV photons as shown later in Fig. 5.

For the low-lying electronic structure, the bands dominated by d_{xz}, d_{yz}, and d_{xy} could be selectively probed in different geometries [Fig. 4(b)]. The α_x band appears in the p geometry, while the β_x band could be observed in the s geometry. The γ_x and δ_x bands show weak photoemission intensities in the s geometry due to the small matrix element of the d_{xy} orbital. These two bands could be observed more clearly in Figs. 5 and 6. We further investigated the photoemission intensity maps at 50 meV below E_F [Fig. 4(c)]. Two ellipse-like features observed in the p and s geometries originate from the d_{xz} and d_{yz} orbitals, respectively. They intertwine with each other forming the cross-sections of the α and β hole pockets. The outmost feature is the γ band cross-section, which is suppressed along the k_x direction in the p geometry, consistent with the matrix element distribution of the d_{xy} orbital. When the sample is cooled down to 20 K, the symmetry breaking of electronic structure is notable on the cross-sections of the α and β hole pockets [Fig. 4(d)]. Both pockets extend along the AFM direction. The d_{yz} portions show more anisotropy than the d_{xz} portions, indicating an orbital-dependent reconstruction of the electronic structure.

IV. THE ELECTRONIC STRUCTURE OF THE NEMATIC STATE

As shown in Sec. III, although the simple matrix element calculation is not quantitative, there is a good qualitative agreement between the prediction and our experimental results. Therefore, NaFeAs provides an ideal opportunity for us to study the temperature dependence of d_{xz}, d_{yz}, and d_{xy} separately along both AFM and FM directions. We will focus on the temperature dependence of the bands that make the electron pockets first.

A. The temperature dependence of the η and δ bands

There are two electron pockets η and δ around the zone corner. The η_x bands could be clearly identified crossing

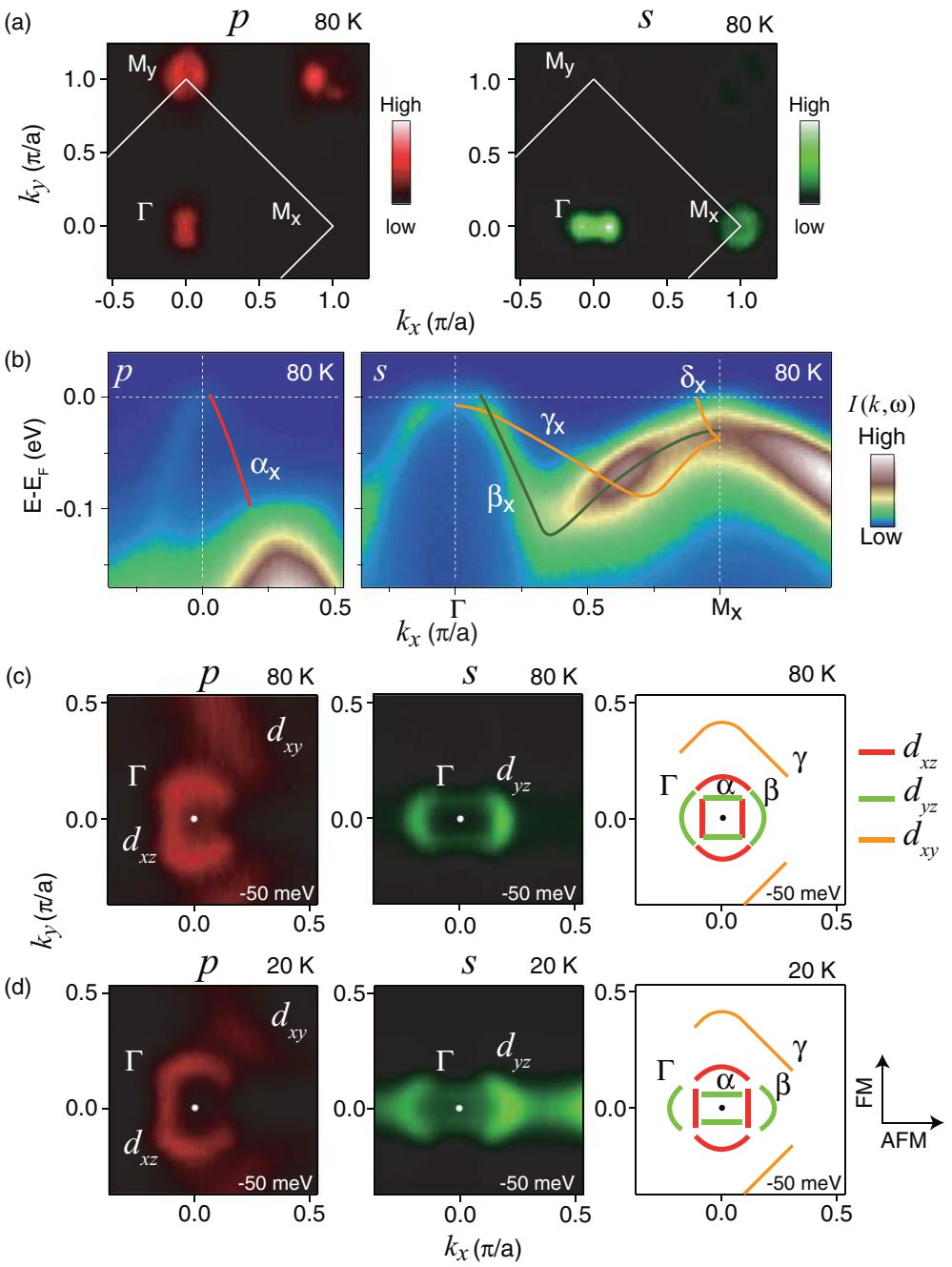

FIG. 4. (Color online) The polarization sensitivity of bands with different orbitals. (a) The photoemission intensity maps integrated over a 10-meV energy window at E_F taken at 80 K in the p and s geometries. (b) The photoemission intensity [$I(k,\omega)$] taken at 80 K in the p and s geometries along Γ-M_x direction. The band dispersions are overlayed on the photoemission intensities with the solid lines. (c) The left and middle panels are the photoemission intensity maps integrated over a 10-meV energy window at 50 meV below E_F taken at 80 K in the p and s geometries, respectively. The observed cross-sections of bands are summarized in the right panel. (d) Same as described for panel (c) but taken at 20 K. All the data were taken with 107-eV photons.

E_F along the k_x direction in the p geometry [Fig. 5(a)]. Their Fermi crossings move outward continuously as the temperature decreases [Fig. 5(b)]. The momentum shift for η_x is about 0.02 π/a from 60 to 20 K. For the δ electron pocket, we took the data along the momentum cut around M_y in the p geometry in order to enhance its photoemission intensity. Note that, the band dispersions along the k_x direction should be equivalent for M_x and M_y, which is protected by the translational symmetry. As shown in Figs. 5(c)–5(e), when the temperature decreases, the MDCs peak intensities of δ_x suppress near E_F promptly, indicating an energy gap opening for the δ_x band along the k_x direction.

Along the k_y direction, the photoemission intensity of η_y is too weak to be distinguished [Fig. 5(f)]. As will be discussed later, this is because the η_y bands shift up above E_F. The tiny MDCs peaks observed in Fig. 5(g) might be due to the

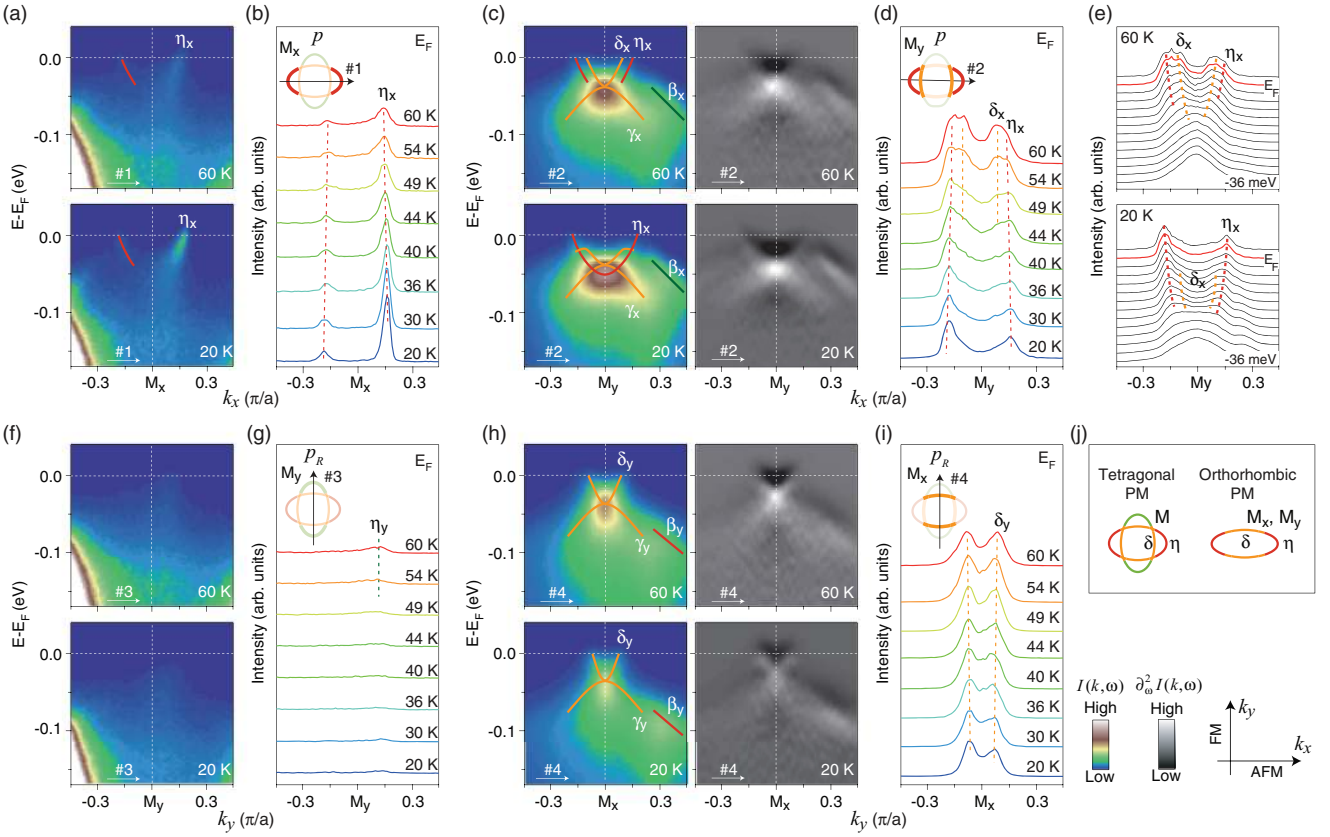

FIG. 5. (Color online) The temperature-dependent photoemission data of the η and δ bands around the zone corner. (a) The $I(k,\omega)$ taken at 60 and 20 K in the p geometry along Cut 1. (b) The temperature dependence of the momentum distribution curves (MDCs) at E_F along Cut 1. The momentum position of Cut 1 is shown by a black arrow in the inset of panel (b). (c) The $I(k,\omega)$ and its second derivative image with respect to energy $[\partial^2 I(k,\omega)/\partial\omega^2]$ taken at 60 and 20 K in the p geometry along Cut 2. (d) The temperature dependence of the MDCs at E_F along Cut 2. The momentum position of Cut 2 is shown by a black arrow in the inset of panel (d). (e) The MDCs selected from -36 meV to 3 meV for the data in panel (a). Each MDCs has been individually normalized by its integrated weight to highlight weak features. (f), (g) Same as described for panels (a) and (b) but taken in the p_R geometry along Cut 3. (h), (i) Same as described for panels (c) and (d) but taken in the p_R geometry along Cut 4. (j) The sketch of the electron pockets in the tetragonal PM and orthorhombic PM states. All the data were taken with 118-eV photons. The color scales of $I(k,\omega)$ and $\partial^2 I(k,\omega)/\partial\omega^2$ are shown in the bottom-right inset. These color scales and notations are used throughout the paper. The band dispersions are overlayed on the photoemission intensities with the solid lines, which are determined with the help of the second derivative images and MDCs.

minor twinned domains of the sample. The δ_y portions of the inner electron pocket show weak temperature dependence [Figs. 5(h) and 5(i)]. The Fermi crossings of δ_y slightly shrink with a momentum shift of about 0.02 π/a from 60 to 20 K.

The observed in-plane anisotropy of the electron pockets preserves at the temperature as high as 60 K, which is far above the structural and magnetic transition temperatures in unstressed sample. This suggests that the reconstruction of the electronic structure might be closely related to the stress and thus lattice distortion, whose onset temperature (T_S') increases due to the uniaxial pressure (More evidences in Fig. 8). Therefore, under the structural transition, the electron pockets reconstruct significantly as shown in Fig. 5(j). Two portions vanish in the orthorhombic PM state and the remaining electron pocket extends along the k_x direction.

B. The temperature dependence of the α, β, and γ bands

To investigate the β and γ bands, temperature-dependent data taken in the s geometry along the k_x direction are shown in Fig. 6(a). Remarkable band reconstruction was observed. Near Γ, the β_x and γ_x bands open a large hybridization gap at 20 K. As a result, the Fermi crossings of β_x are pushed outward from Γ, and the band top of γ shifts downward to about 40 meV below E_F [Figs. 6(a), 6(b), and 6(d)]. The β_x band disperses toward E_F around M forming a hole-like band. It hybridizes with the δ_x electron pocket and opens an energy gap at E_F upon lowing the temperature. This is consistent with the gap opening of δ_x observed in Figs. 5(c)–5(e). Moreover, the band shift and hybridization push the β_x band above E_F around M. Considering the fact that the β_x band should connect with the band bottom of η_y [Fig. 3(c)], we could further confirm the observation in Fig. 5(f) that the η_y portions of the outer electron pocket shift up above E_F in the orthorhombic PM state. Note that the long-range magnetic order could halve the Brillouin zone by folding the bands between Γ and M. We thus attributed η_x' near Γ together with β_x' and α_x' around M to be the folded bands in the magnetic state.

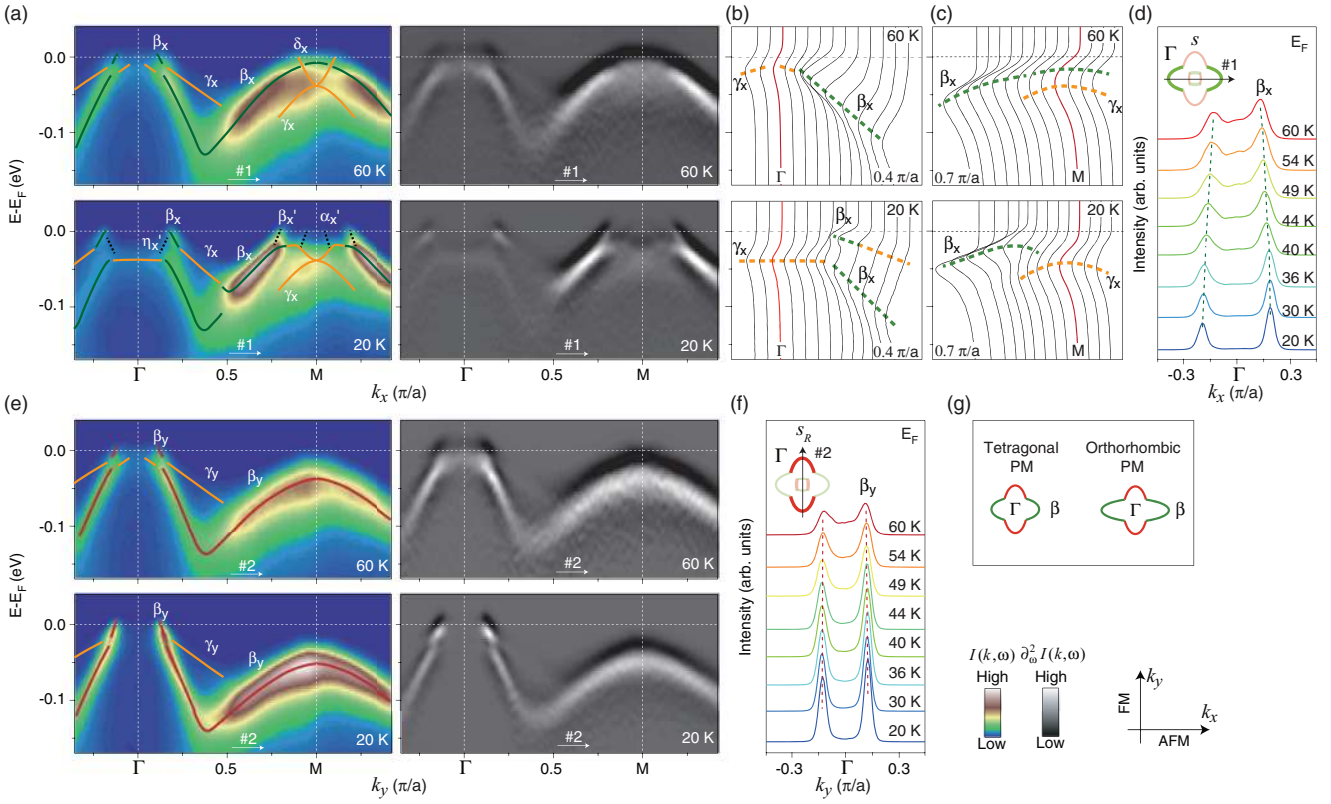

FIG. 6. (Color online) The temperature-dependent photoemission data of the β and γ bands. (a) The $I(k,\omega)$ and $\partial^2 I(k,\omega)/\partial\omega^2$ taken at 60 and 20 K in the s geometry along Cut 1. (b), (c) The energy distribution curves (EDCs) for the data in panel (a) selected around Γ and M, respectively. (d) The temperature dependence of the MDCs at E_F along Cut 1. The momentum position of Cut 1 is shown by a black arrow in the inset of panel (d). (e), (f) Same as described for panels (a) and (d) but taken in the s_R geometry along Cut 2. (g) The sketch of the β hole pocket in the tetragonal PM and orthorhombic PM states. All the data were taken with 118-eV photons.

In contrast to the complex behavior along k_x, the β band does not reconstruct along the k_y direction [Fig. 6(e)]. The Fermi crossings of β_y are almost temperature independent as shown in Fig. 6(f). Around the M point, the β_y band shifts downward to about -50 meV at the lowest temperature. Since β_y should connect with the band bottom of η_x [Fig. 3(d)], such an energy shift of β_y is consistent with the enlargement of η_x observed in Fig. 5(a). We summarized the reconstruction of β in Fig. 6(g). The β hole pocket extends along the AFM direction in the orthorhombic PM state.

The reconstruction of the inner α hole pocket is shown in Fig. 7. Along the k_y direction, the α_y band splits into two parts, indicating possible hybridization with other bands [Figs. 7(a) and 7(c)]. The hybridization with δ_y' could be first excluded. According to the temperature-dependent data, while band shift of the lower part of α_y is notable at 60 K [Fig. 7(d)], the folding of δ_y occurs at a much lower temperature of about 49 K [Fig. 7(b)]. Moreover, no hybridization was found for the δ_y band in Fig. 5(h). Therefore, the α_y band should hybridize strongly with the γ_y band in the orthorhombic PM state, as shown in the inset of Fig. 7(c). In this case, a large proportion of the d_{yz} orbital on α_y would be mixed into γ_y due to such hybridization. Consequently, we note that the photoemission intensity of γ_y is suppressed at 20 K around the Γ point in Fig. 6(e), as the d_{yz} orbital could not be observed in the s_R geometry. Along the k_x direction, the α_x bands show weak temperature dependence. Their Fermi crossings slightly move outward about $0.02\ \pi/a$ from 60 to 20 K [Figs. 7(e)–7(g)]. Therefore, similar to the β hole pocket, the α hole pocket extends along the AFM direction in the orthorhombic PM state as shown in Fig. 7(h).

Our previous APRES study on twinned NaFeAs has found that the short range magnetic order emerges just below the structural transition temperature of 54 K, which causes a band folding.[24] However, when the structural transition is enhanced to 75 K here by the uniaxial pressure, we still observe the folding of δ_y bands below $\sim$49 K [Fig. 7(b)]. Therefore, the short-range magnetic order observed above T_N in previous study should be related to the fluctuation of the long-range magnetic order, instead of a direct correlation with the structural transition.

V. DISCUSSION

To further investigate the orbital-dependent behaviors of the reconstruction in the orthorhombic PM state, the bands dominated by the d_{yz} and d_{xy} orbitals are highlighted in Fig. 8(a). The most remarkable feature found here is the hybridization gap opening at almost all band crossings. As a result, the bands split into the upper and lower bands around Γ and open an energy gap at E_F around M. Such reconstruction could redistribute the orbital weight of d_{yz} and d_{xy}, inducing a

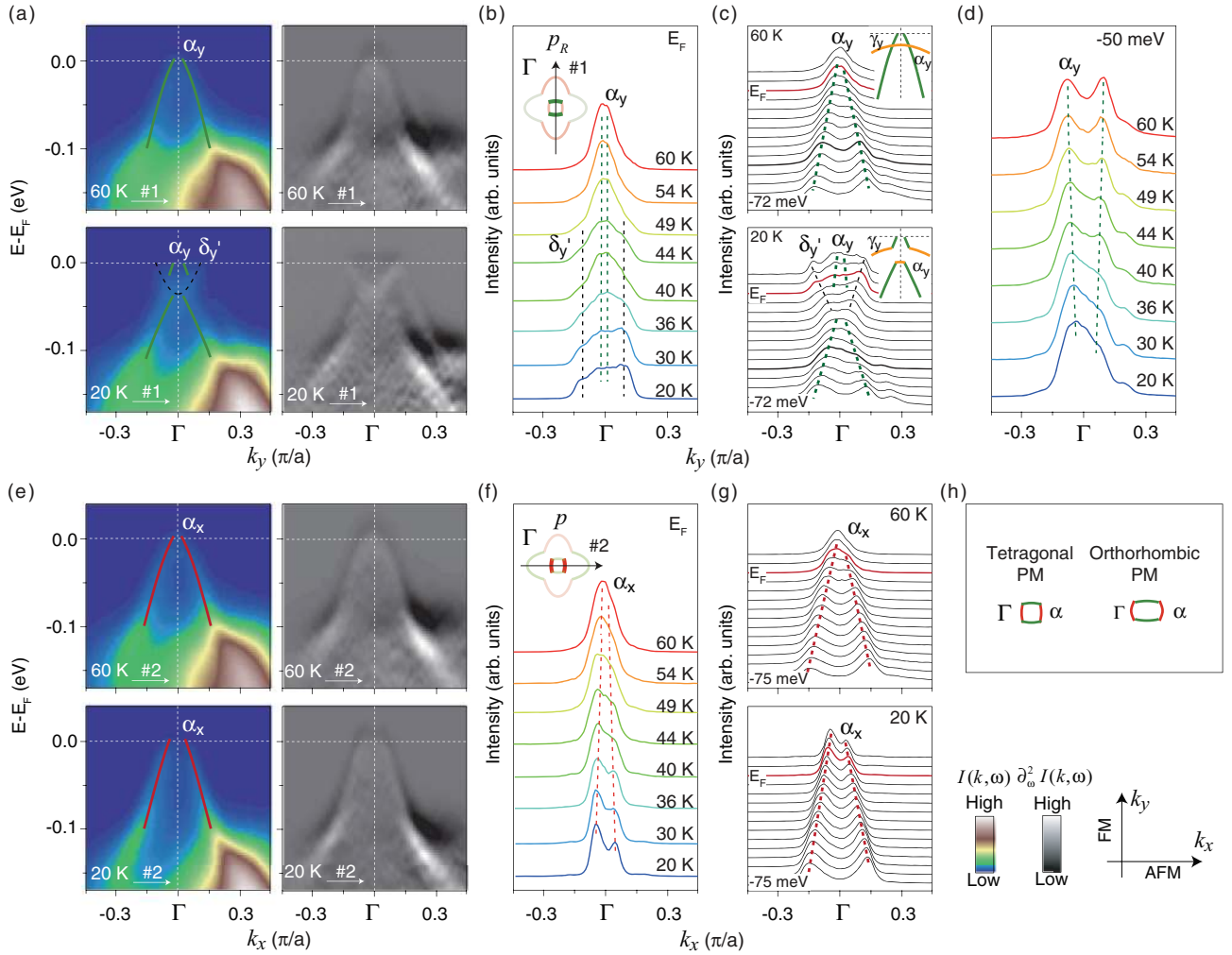

FIG. 7. (Color online) The temperature-dependent photoemission data of the α band around the zone center. (a) The $I(k,\omega)$ and $\partial^2 I(k,\omega)/\partial\omega^2$ taken at 60 and 20 K in the p_R geometry along Cut 1. (b) The temperature dependence of the MDCs at E_F along Cut 1. The momentum position of Cut 1 is shown by a black arrow in the inset of panel (b). (c) The MDCs selected from −72 to 12 meV for the data in panel (a). Each MDC has been individually normalized by its integrated weight to highlight weak features. (d) The temperature dependence of the MDCs at 50 meV below E_F along Cut 1. (e), (f), and (g) Same as described for panels (a), (b), and (c) but taken in the p geometry along Cut 2. (h) The sketch of the α hole pocket in the tetragonal PM and orthorhombic PM states. All the data were taken with 118-eV photons.

partial gap near the Fermi energy [Fig. 8(b)]. On the contrary, the d_{xz}-dominated bands exhibit no remarkable reconstruction, except an energy shift around M [Fig. 8(c)]. The orbital weight redistribution is negligible for the d_{xz} orbital. Furthermore, since the energy shifts of β_x and β_y are pronounced near the M point, we use such energy shift as a parameter to describe the reconstruction of the electronic structure. If the C_4 rotational symmetry of the electronic structure is preserved, the β band dominated by the d_{xz} and d_{yz} orbitals should degenerate along the k_x and k_y directions. As shown in Figs. 8(d)–8(f), when the temperature decreases, the energy splitting between β_x and β_y bands enlarges linearly and almost saturates at T_N. The onset temperature of such splitting could be estimated to be around 75 K, where the in-plane anisotropy of resistivity emerges (T_S'). This result is consistent with previous study on the "122" series of iron pnictides,[12] and suggests that the orbital weight redistribute significantly under the structural transition. Moreover, the smooth evolution of the electronic structure reconstruction into the CAF state indicates that both the magnetic and structural transitions share the same driving force.[24]

So far, there are mainly two categories of theoretical proposals for understanding the origin of the nematic electronic ordered state above T_N. One category of theories suggests that the nematicity could originate from spin fluctuations.[17–19] The spin fluctuations could couple with the nematic electronic order and break the lattice symmetry via electron-lattice coupling.[17] The other category of theories suggests that the orbital degree of freedom could be dominating. Different types of orbital ordering were proposed to be accompanied by the magnetic order.[20] Especially, the ferro-orbital ordering originated from the inequivalent occupations of d_{xz} and d_{yz} was proposed to drive the structural transition and stabilize the long-range magnetic order.[21–23] Our results provide several important quantitative tests for these theoretical proposals. We could first check the inequivalent occupation between the

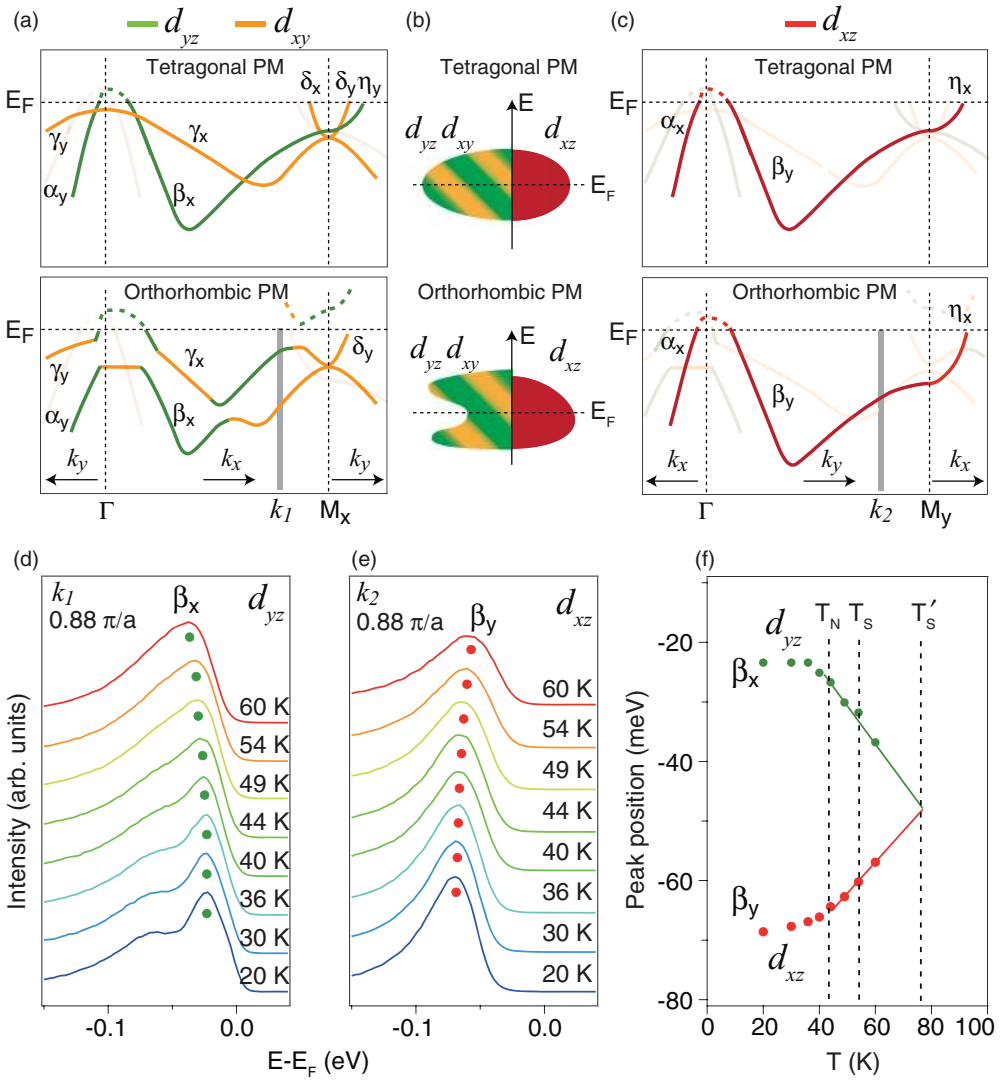

FIG. 8. (Color online) The orbital-dependent reconstruction of the electronic structure. (a) The low-lying electronic structure in the tetragonal PM and orthorhombic PM state, respectively, where only the d_{yz}- and d_{xy}-dominated bands are highlighted. The band dispersions above E_F are shown by dashed lines, considering the continuous dispersion of the bands with certain orbitals. (b) Cartoon shows the orbital weight distributions near E_F in the tetragonal PM and orthorhombic PM states. (c) The low-lying electronic structure in the tetragonal PM and orthorhombic PM state, respectively, where only the d_{xz}-dominated bands are highlighted. (d) The temperature dependence of the EDCs at k_1 as indicated by the gray line in panel (a). (e) The temperature dependence of the EDCs at k_2 as indicated by the gray line in panel (c). (f) The peak positions of the β_x and β_y bands as functions of temperature.

d_{xz} and d_{yz} orbitals, which is considered to be important for the formation of ferro-orbital ordering.[21–23] The occupation change of the d_{xz} orbital could be calculated from the size increase of the η_x electron pocket subtracted by the size increase of the α_x hole pocket. The momentum shift of the η_x Fermi crossings is about 0.02 π/a from 60 to 20 K. Considering the band shift above 60 K [Fig. 8(f)], this momentum shift might be doubled to 0.04 π/a, corresponding to a maximum occupation change of about 0.04 electron per iron. Moreover, the Fermi momenta variations are almost the same for the enlargement of the η_x electron pocket and the α_x hole pocket. Therefore, *the occupation change of the d_{xz} orbital should be infinitesimal*, which suggests that the ferro-orbital ordering only involving d_{xz} and d_{yz} plays a minor role in driving the nematic transitions here.[21] Note that, although the occupation of d_{xz} is almost invariant, the orbital polarization could be strong only at the low energy. Since the orbital weight of d_{yz} and d_{xy} is partially gaped away from E_F, the Fermi surface could be dominated by the d_{xz} orbital in the orthodromic state.[16,37]

More intriguingly, instead of the pure ferro-orbital ordering between d_{xz} and d_{yz} orbitals, the reconstruction of the electronic structure involves mostly the d_{yz} and d_{xy} orbitals. These two orbitals are found numerically to contribute much larger magnetic moment than d_{xz} in the magnetic ordered state.[22,34–37] Therefore, the orbital weight redistribution observed here below T_S' could be related to the spin polarization of the d_{yz} and d_{xy} orbitals. In this scenario, the strong coupling between spin fluctuations and the orbital degree of freedom could induce an orbital-dependent spin polarization far above

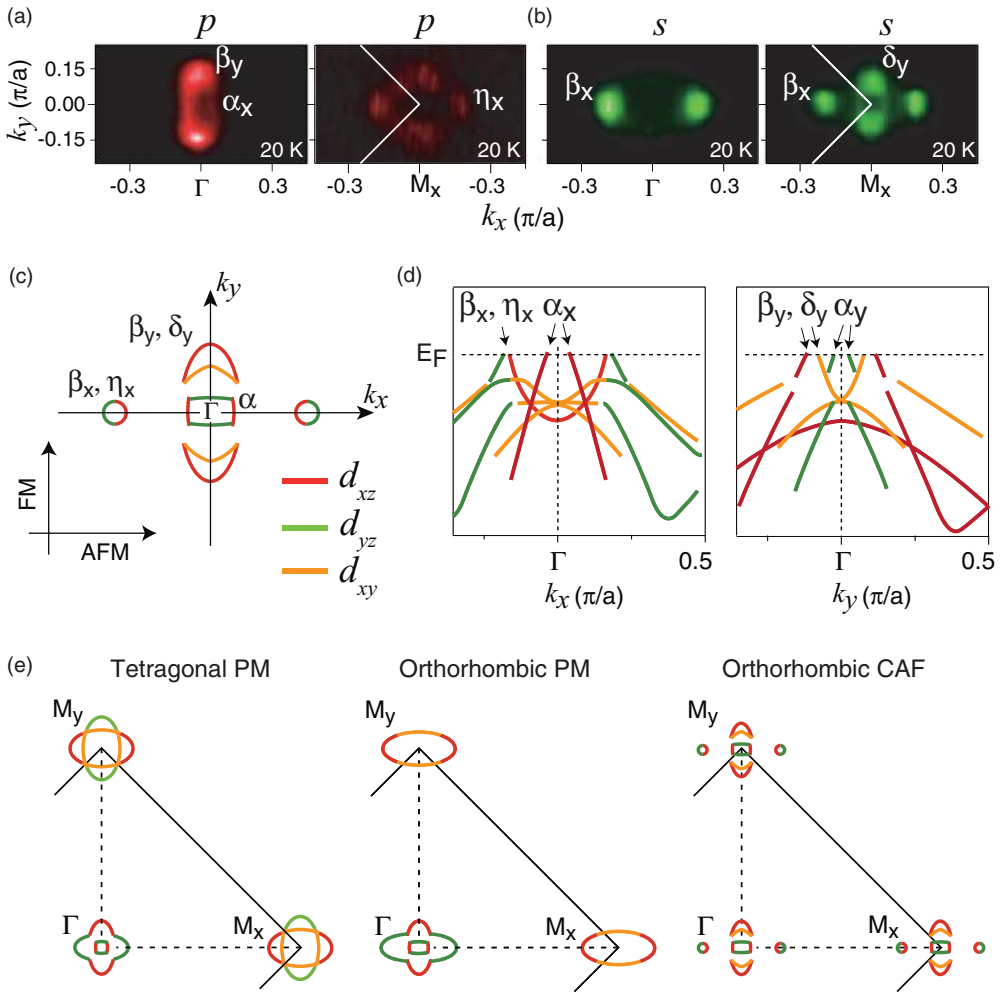

FIG. 9. (Color online) The temperature dependence of the Fermi surface morphology. (a) The photoemission intensity maps in the orthorhombic CAF state taken around Γ and M in the p geometry. (b) Same as described for panel (a) but taken in the s geometry. The intensity was integrated over a 10-meV energy window at E_F. (c) The Fermi surface morphology in the orthorhombic CAF state. (d) The band structure along k_x and k_y directions in the orthorhombic CAF state. (e) The summary of Fermi surfaces in the tetragonal PM, orthorhombic PM, and orthorhombic CAF state, respectively.

the Neel temperature, which further reinforces the spin fluctuations and the nematicity of electronic structure. Such a positive feedback process can break the C4 rotational symmetry and thus induce the structural transition. Consistently, the enhancement of spin fluctuations was observed below the structural transition temperature.[38] Our results therefore suggest that the nematic spin fluctuations at high temperatures and their coupling with the orbital degree of freedom could be the dominating cause for the nematic electronic state in the iron pnictides. Note that the feedback process could be further accelerated by an uniaxial stress. It thus could explain the dramatic enhancement of T_S by the rather small pressure applied in our experiment.[8]

In the magnetic state, the electronic structure is folded between Γ and M due to the long-range magnetic order. According to the photoemission intensity maps in the s and p geometries [Figs. 9(a) and 9(b)], the Fermi surface morphology and the band structure in the orthorhombic CAF state are shown in Figs. 9(c) and 9(d). The electron pocket folds from M to Γ and then hybridizes with the β hole pocket. As a result, four small pockets are formed. There are two bright spots along AFM direction dominated by the d_{yz} and d_{xz} orbitals. Since they are formed by two bands with opposite symmetries [Figs. 9(c) and 9(d)], these two small pockets are intensively discussed as Dirac points in 122 series.[12,39,40] The other two pockets are formed by the δ_y and β_y bands along the FM direction [Figs. 9(c) and 9(d)].

We summarized the reconstruction of Fermi surface in Fig. 9(e). The C_4 rotational symmetry of the Fermi surface is broken under the structural transition. The anisotropic Fermi surface observed in the orthorhombic PM state could be responsible for the in-plane anisotropic transport behaviors above T_N.[8–10,41] All the pockets show anisotropic shape with an extension along the k_x direction. Especially, the transport properties contributed by the electron pockets could be highly anisotropic, since two portions of electron pockets are gaped away from E_F in the orthorhombic PM state. When entering the orthorhombic CAF state, the Fermi pockets are folded

between Γ and M. The Fermi surface is thus characterized by four distinct pockets originated from the hybridization between the hole and electron pockets. These features qualitatively agree with previous studies in the 122-series,[11,12,15,35] which highlight the unified nature of the nematic magnetic state in iron pnictides. Furthermore, the Fermi crossings of β, δ_y, and η_x are sensitive to the structures, k_z, and doping levels. Therefore, the topology of these four pockets could be variable in different compounds. For example, the pockets distributed along FM direction are hole-like in NaFeAs, but electron-like in 122 series.[11,12,15,35] In that case, the topology change of these distinct features could be responsible for the nonmonotonic doping dependence of the in-plane resistivity anisotropy observed in 122 series.[8–10,42]

VI. SUMMARY

To summarize, our polarization-dependent ARPES study on detwinned NaFeAs clearly demonstrates the details of the electronic structure reconstruction in the nematic state. We found that the rotational symmetry breaking of electronic structure is closely related to the in-plane anisotropy of the resistivity, whose onset temperature is far above the Neel transition temperature. More intriguingly, such a symmetry breaking originates from the reconstruction of the electronic structure and exhibits orbital-dependent behaviors. The d_{yz}- and d_{xy}-dominated bands split near Γ and open an energy gap around M, while the d_{xz}-dominated bands only exhibit an energy shift without any reconstruction. Our observations exclude the theories based on the ferro-orbital ordering only involving the d_{xz} and d_{yz} orbitals, since the occupation of d_{xz} is almost temperature independent. Instead, the strong coupling between the nematic spin fluctuations and the orbital degree of freedom are suggested to drive the nematicity. Such a coupling causes an orbital-dependent spin polarization, and thus the development of finite magnetic moments of the d_{yz} and d_{xy} orbitals as manifested in their weight redistributions. Our findings provide the experimental foundation for a microscopic understanding of the nematic state of iron pnictides.

ACKNOWLEDGMENTS

We thank Dr. Chi-Cheng Lee for helpful discussions and Dr. Dong-hui Lu. and Dr. Changyoung Kim for sharing experiences of the mechanically detwinning method. This work is supported in part by the National Science Foundation of China, Ministry of Education of China, Science and Technology Committee of Shanghai Municipal, Key discipline innovation talents cultivation program of Fudan University, and National Basic Research Program of China (973 Program) under Grant Nos. 2011CB921802, 2011CBA00112, and 2012CB921400.

*dlfeng@fudan.edu.cn

[1] C. de la Cruz, Q. Huang, J. W. Lynn, J. Li, W. R. Ii, J. L. Zarestky, H. A. Mook, G. F. Chen, J. L. Luo, N. L. Wang, and P. Dai, Nature (London) **453**, 899 (2008).

[2] Q. Huang, Y. Qiu, W. Bao, M. A. Green, J. W. Lynn, Y. C. Gasparovic, T. Wu, G. Wu, and X. H. Chen, Phys. Rev. Lett. **101**, 257003 (2008).

[3] S. Li, C. de la Cruz, Q. Huang, G. F. Chen, T. L. Xia, J. L. Luo, N. L. Wang, and P. Dai, Phys. Rev. B **80**, 020504 (2009).

[4] J. Zhao, Q. Huang, C. de la Cruz, S. Li, J. W. Lynn, Y. Chen, M. A. Green, G. F. Chen, G. Li, Z. Li, J. L. Luo, N. L. Wang, and P. Dai, Nat. Mater. **7**, 953 (2008).

[5] M. Rotter, M. Tegel, and D. Johrendt, Phys. Rev. Lett. **101**, 107006 (2008).

[6] M. S. Torikachvili, S. L. Budko, N. Ni, and P. C. Canfield, Phys. Rev. Lett. **101**, 057006 (2008).

[7] J. Zhao, D. T. Adroja, D.-X. Yao, R. Bewley, S. Li, X. F. Wang, G. Wu, X. H. Chen, J. Hu, and P. Dai, Nature Physics **5**, 555 (2009).

[8] J.-H. Chu, J. G. Analytis, K. De Greve, P. L. McMahon, Z. Islam, Y. Yamamoto, and I. R. Fisher, Science **329**, 824 (2010).

[9] J. J. Ying, X. F. Wang, T. Wu, Z. J. Xiang, R. H. Liu, Y. J. Yan, A. F. Wang, M. Zhang, G. J. Ye, P. Cheng, J. P. Hu, and X. H. Chen, Phys. Rev. Lett. **107**, 067001 (2011).

[10] H.-H. Kuo, J.-H. Chu, S. C. Riggs, L. Yu, P. L. McMahon, K. De Greve, Y. Yamamoto, J. G. Analytis, and I. R. Fisher, Phys. Rev. B **84**, 054540 (2011).

[11] Q. Wang, Z. Sun, E. Rotenberg, F. Ronning, E. D. Bauer, H. Lin, R. S. Markiewicz, M. Lindroos, B. Barbiellini, A. Bansil, and D. S. Dessau, e-print arXiv:1009.0271.

[12] M. Yi, D. Lu, J.-H. Chu, J. G. Analytis, A. P. Sorini, A. F. Kemper, B. Moritz, S.-K. Mo, R. G. Moore, M. Hashimoto, W.-S. Lee, Z. Hussain, T. P. Devereaux, I. R. Fisher, and Z.-X. Shen, Proc. Nat. Acad. Sci. USA **108**, 6878 (2011).

[13] Y. Kim, H. Oh, C. Kim, D. Song, W. Jung, B. Kim, H. J. Choi, C. Kim, B. Lee, S. Khim, H. Kim, K. Kim, J. Hong, and Y. Kwon, Phys. Rev. B **83**, 064509 (2011).

[14] T.-M. Chuang, M. P. Allan, J. Lee, Y. Xie, N. Ni, S. L. Bud'ko, G. S. Boebinger, P. C. Canfield, and J. C. Davis, Science **327**, 181 (2010).

[15] T. Terashima, N. Kurita, M. Tomita, K. Kihou, C.-H. Lee, Y. Tomioka, T. Ito, A. Iyo, H. Eisaki, T. Liang, M. Nakajima, S. Ishida, S.-i. Uchida, H. Harima, and S. Uji, Phys. Rev. Lett. **107**, 176402 (2011).

[16] T. Shimojima, K. Ishizaka, Y. Ishida, N. Katayama, K. Ohgushi, T. Kiss, M. Okawa, T. Togashi, X. Y. Wang, C. T. Chen, S. Watanabe, R. Kadota, T. Oguchi, A. Chainani, and S. Shin, Phys. Rev. Lett. **104**, 057002 (2010).

[17] C. Fang, H. Yao, W.-F. Tsai, J. P. Hu, and S. A. Kivelson, Phys. Rev. B **77**, 224509 (2008).

[18] F. Ma, Z.-Y. Lu, and T. Xiang, Phys. Rev. B **78**, 224517 (2008).

[19] I. I. Mazin and M. D. Johannes, Nature Physics **5**, 141 (2009).

[20] F. Kruger, S. Kumar, J. Zaanen, and J. van den Brink, Phys. Rev. B **79**, 054504 (2009).

[21] W. Lv, J. Wu, and P. Phillips, Phys. Rev. B **80**, 224506 (2009).

[22] C.-C. Lee, W.-G. Yin, and W. Ku, Phys. Rev. Lett. **103**, 267001 (2009).

[23] C.-C. Chen, J. Maciejko, A. P. Sorini, B. Moritz, R. R. P. Singh, and T. P. Devereaux, Phys. Rev. B **82**, 100504(R) (2010).

[24]C. He, Y. Zhang, B. P. Xie, X. F. Wang, L. X. Yang, B. Zhou, F. Chen, M. Arita, K. Shimada, H. Namatame, M. Taniguchi, X. H. Chen, J. P. Hu, and D. L. Feng, Phys. Rev. Lett. **105**, 117002 (2010).

[25]M. A. Tanatar, E. C. Blomberg, A. Kreyssig, M. G. Kim, N. Ni, A. Thaler, S. L. Budko, P. C. Canfield, A. I. Goldman, I. I. Mazin, and R. Prozorov, Phys. Rev. B **81**, 184508 (2010).

[26]G. F. Chen, W. Z. Hu, J. L. Luo, and N. L. Wang, Phys. Rev. Lett. **102**, 227004 (2009).

[27]E. C. Blomberg, A. Kreyssig, M. A. Tanatar, R. Fernandes, M. G. Kim, A. Thaler, J. Schmalian, S. L. Bud'ko, P. C. Canfield, A. I. Goldman, and R. Prozorov, e-print arXiv:1111.0997.

[28]C. Dhital, Z. Yamani, W. Tian, J. Zeretsky, A. S. Sefat, Z. Wang, R. J. Birgeneau, and S. D. Wilson, e-print arXiv:1111.2326.

[29]A. Damascelli, Z. Hussain, and Z.-X. Shen, Rev. Mod. Phys. **75**, 473 (2003).

[30]Y. Zhang, F. Chen, C. He, B. Zhou, B. P. Xie, C. Fang, W. F. Tsai, X. H. Chen, H. Hayashi, J. Jiang, H. Iwasawa, K. Shimada, H. Namatame, M. Taniguchi, J. P. Hu, and D. L. Feng, Phys. Rev. B **83**, 054510 (2011).

[31]S. Graser, T. A. Maier, P. J. Hirschfeld, and D. J. Scalapino, New J. Phys. **11**, 025016 (2009).

[32]K. Kusakabe and A. Nakanishi, J. Phys. Soc. Jpn. **78**, 124712 (2009).

[33]C. He, Y. Zhang, X. F. Wang, J. Jiang, F. Chen, L. X. Yang, Z. R. Ye, F. Wu, M. Arita, K. Shimada, H. Namatame, M. Taniguchi, X. H. Chen, B. P. Xie, and D. L. Feng, J. Phys. Chem. Solids. **72**, 479 (2011).

[34]H. Oh, D. Shin, and H. J. Choi, e-print arXiv:1012.2224.

[35]Z. P. Yin, K. Haule, and G. Kotliar, Nature Physics **7**, 294 (2011).

[36]Z. P. Yin and W. E. Pickett, Phys. Rev. B **81**, 174534 (2010).

[37]M. Daghofer, Q. Luo, R. Yu, D. Yao, A. Moreo, and E. Dagotto, e-print arXiv:1004.4803.

[38]L. Ma, G. F. Chen, D.-X. Yao, J. Zhang, S. Zhang, T. L. Xia, and W. Yu, Phys. Rev. B **83**, 132501 (2011).

[39]P. Richard, K. Nakayama, T. Sato, M. Neupane, Y. M. Xu, J. H. Bowen, G. F. Chen, J. L. Luo, N. L. Wang, X. Dai, Z. Fang, H. Ding, and T. Takahashi, Phys. Rev. Lett. **104**, 137001 (2010).

[40]T. Morinari, E. Kaneshita, and T. Tohyama, Phys. Rev. Lett. **105**, 037203 (2010).

[41]A. Dusza, A. Lucarelli, F. Pfuner, J.-H. Chu, I. R. Fisher, and L. Degiorgi, Eur. Phys. Lett. **93**, 37002 (2011).

[42]B. Valenzuela, E. Bascones, and M. J. Calderon, Phys. Rev. Lett. **105**, 207202 (2010).